Chapter 8

Optimized Negative-Staining Protocol for Lipid–Protein Interactions Investigated by Electron Microscopy

Jianfang Liu, Hao Wu, Changyu Huang, Dongsheng Lei, Meng Zhang, Wei Xie, Jinping Li, and Gang Ren

Abstract

A large number of proteins are capable of inserting themselves into lipids, and interacting with membranes, such as transmembrane proteins and apolipoproteins. Insights into the lipid-protein interactions are important in understanding biological processes, and the structure of proteins at the lipid binding stage can help identify their roles and critical functions. Previously, such structural determination was challenging to obtain because the traditional methods, such as X-ray crystallography, are unable to capture the conformational and compositional heterogeneity of protein–lipid complexes. Electron microscopy (EM) is an alternative approach to determining protein structures and visualizing lipid–protein interactions directly, and negative-staining (OpNS), a subset of EM techniques, is a rapid, frequently used qualitative approach. The concern, however, is that current NS protocols often generate artifacts with lipid-related proteins, such as rouleaux formation from lipoproteins. To overcome this artifact formation, Ren and his colleagues have refined early NS protocols, and developed an optimized NS protocol that validated by comparing images of lipoproteins from cryo-electron microscopy (cryo-EM). This optimized NS protocol produces "near native-state" particle images and high contrast images of the protein in its native lipid-binding state, which can be used to create higher-quality three-dimensional (3D) reconstruction by single-particle analysis and electron tomography (e.g. IPET). This optimized protocol is thus a promising hands-on approach for examining the structure of proteins at their lipid-binding status.

Key words Lipoprotein structure, Lipoprotein morphology, Electron microscopy, Optimized negative-staining protocol, Negative-staining electron microscopy

1 Introduction

Lipid-protein interactions can be found between the membrane proteins and/or apolipoproteins and lipids, which can function as pumps, transporters, cell-to-cell communication messengers [1], or lipid transfer vehicles for lipid metabolism [2]. To understand the function of these biological complexes, studying the structure of a protein at the lipid-binding stage is crucial. Due to the differences in size, shape, and the lipid components, determining its structure is extremly tedious. However, the dynamic nature of lipoproteins

Jörg H. Kleinschmidt (ed.), *Lipid-Protein Interactions: Methods and Protocols*, Methods in Molecular Biology, vol. 2003, https://doi.org/10.1007/978-1-4939-9512-7_8,

plays a vital role for cholesteryl transport in cardiovascular disease (CVD).

Structural determination of proteins at the lipid-binding stage is difficult to achieve by X-ray crystallography because of the compositional heterogeneity and conformational alterations of the proteins. Electron Microscopy (EM) is an alternative approach that has been used more frequently to determine protein structure. Among various EM techniques, cryo-crystallography has been successfully applied in determining the "native-state" structure of proteins in the lipid-bound form under frozen conditions [3]. However, this technique is quite difficult to perform because it requires advanced level of equipment, expertise, and most importantly, two-dimensional (2D) crystallization of the proteins, which is still considered a piece of art rather than a native structure.

Single-particle cryo-EM is another alternative approach that has become a popular method used to study protein structure at near atomic resolution [4, 5]. It is used as the only technology capable of directly visualizing proteins at the native state. Due to the radiation damage, cryo-EM imaging is performed under a low-illumination dose and low-temperature conditions. As a result, images contain a relatively low signal-to-noise ratio [6]. By using single-particle cryo-EM, the images of hundreds to thousands of particles embedded in vitreous ice were obtained, and are then grouped and averaged to reduce the noise and increase image contrast before being reconstructed into an averaged 3D map [7, 8]. Usually, this averaging process improves the image contrast [9, 10], while at times it is not an useful approach to obtain high quality images on certain different types of proteins with heterogeneous features [11], such as high-density lipoprotein (HDL), antibodies, and DNA.

Negative staining (NS) is a well-established approach frequently used in many research laboratories. NS-EM can be used to directly visualize individual particles, such as proteins, viruses, and even very thin cell slice specimens. It also facilitates the study of morphology and structure of these particles, along with lipid-binding forms of apolipoprotein [11–15]. NS is more resistant to radiation compared to cryo-EM [12] and has a much higher contrast [13, 14]. A disadvantage of NS is that, however, the protocols are differ from one another, such as using different staining reagents, different dilution buffer and procedures to prepare the specimens. Usually, it can generate the artifacts such as rouleaux in lipid-related samples [16–19]. For example, phosphotungstic acid (PTA) is used in conventional NS at high salt concentrations in buffer, but NS experiments with the apoE4-palmitoyl-oleoylphosphatidylcholine (POPC) phospholipid particle and liposome vesicles showed that the particles were stacked together by PTA connected by lipid surfaces of neighboring particles [11]. As a result, Ren and his colleagues refined the NS protocols and developed an optimized NS (PoNS) protocol that minimizes rouleaux

formation usually seen in the conventional NS-EM studies. Furthermore, this method was utilized to report the structure and morphology of apoE4-POPC [11], reconstituted HDL (rHDL) apoA-I 7.8-nm [12], 8.4-nm [12], 9.6-nm discoidal rHDL [12, 20–25], 9.3-nm spherical rHDL [12], human plasma HDL [26–30], low-density lipoprotein (LDL) [26, 30–32], intermediate-density lipoprotein (IDL) [12, 28, 29], very low-density lipoprotein (VLDL) [12], a hydrophobic glycoprotein such as, 53 kDa cholesteryl ester transfer protein (CETP) [26–30, 33–35], DNA complexes [36–38], RNA complexes [39], neuron proteins [40–44], and the antibody IgG [20, 32, 34, 45–51] (Fig. 1). In comparing to conventional NS protocol, OpNS specifically used following procedures, (1) 1% (w/v) uranyl formate (UF) as negative staining reagent, (2) 0.02 μm filtered the staining reagent right before using it, (3) Dulbecco's phosphate-buffered saline (DPBS) as dilution buffer, which specifically removed the Mg^{2+} and Ca^{2+}, (4) water washing step included, (5) staining process being conducted in dark to avoid the precipitation of UF under light, (6) drying the sample under N2 gas to avoid potential sample deformation. As a result, the OpNS protocol allows the study of morphology and structure of individual particles by minimizing the rouleaux formation and increasing image resolution in 2D structures, which is highly cooperative for subsequential 3D reconstruction models.

The following OpNS protocol is refined from the conventional NS [13], which eliminates rouleaux artifacts of lipoprotein particles, and has been statistically validated as a method to determine lipoprotein particle shapes and sizes [11, 12, 28]. It is performed by placing a drop of the lipoprotein solution on a glow-discharged carbon-coated copper grid and then removing the excess solution by blotting with filter paper (Fig. 2). Immediately after three washes with deionized water, the EM carbon-coated grid (Fig. 2) is stained with uranyl formate (UF) three times (Fig. 2). Following the staining, the grid is blotted again with filter paper, and then air-dried. Since the UF solution is light sensitive and unstable, this step of operation should be performed in the dark [11, 12]. Finally, the prepared grid is stored at room temperature before being used for EM imaging [11, 12] (Fig. 2).

2 Materials

1. Uranyl formate: $UO_2(CHO_2)_2 \cdot H_2O$.
2. 1 NORM-JECT 1 mL Tuberculin: Syringe, Luer.
3. Sterile syringe filter: pore size of 0.02 μm (Anotop 10).
4. Protein sample, 2.5 μL (~0.005 mg/mL, protein).
5. Dulbecco's Phosphate Buffered Saline.

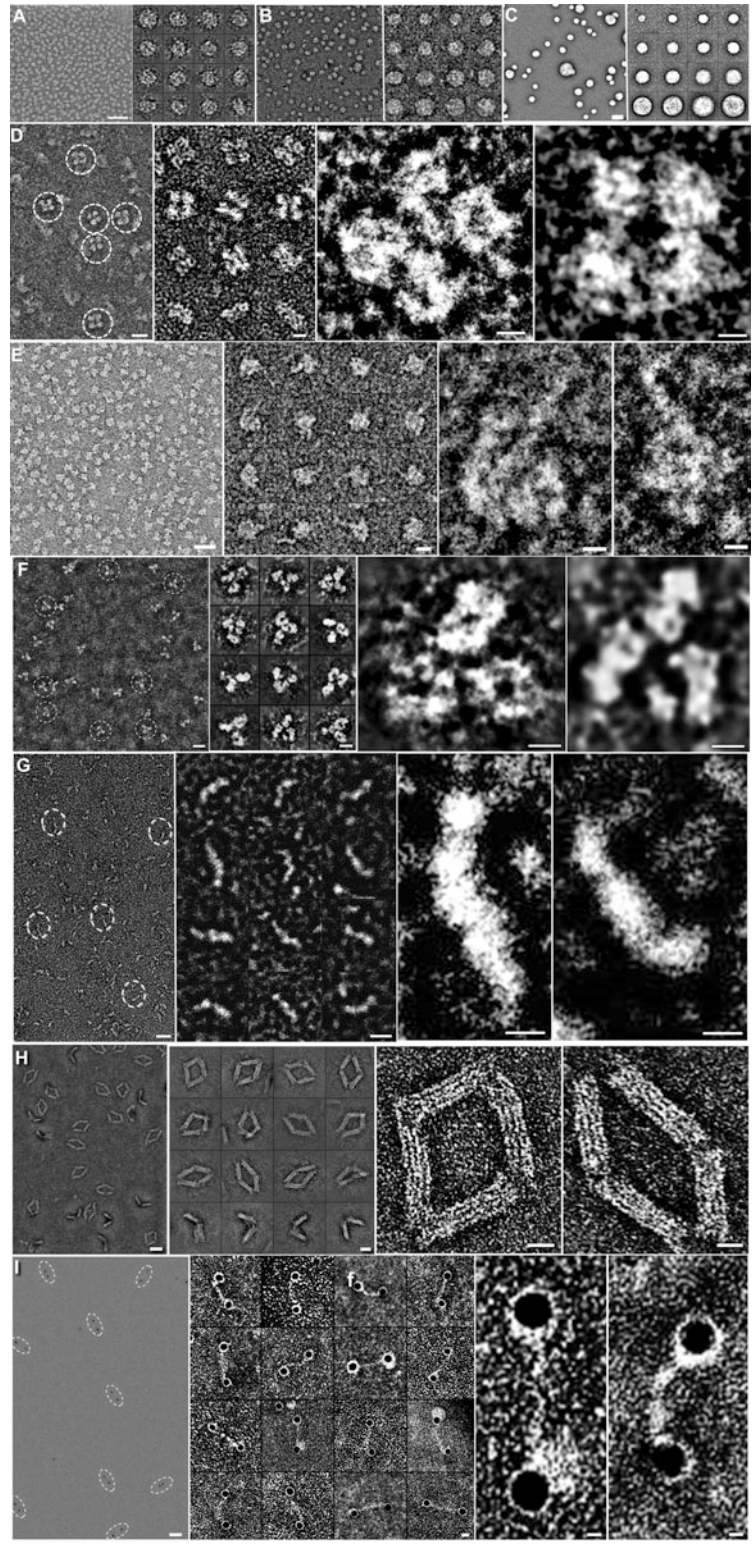

Fig. 1 Morphology of macromolecules by optimized negative-staining EM. Micrographs of apoE4-POPC (**A**), α-HDL from plasma (**B**), VLDL (**C**), Calsyntenin-3 (**D**), Glycyl-tRNA Synthetase (hGlyRS) (**E**), the IgG antibody (**F**), Cholesteryl ester transfer protein (CETP, 53 kDa) (**G**), DNA origami (**H**) and

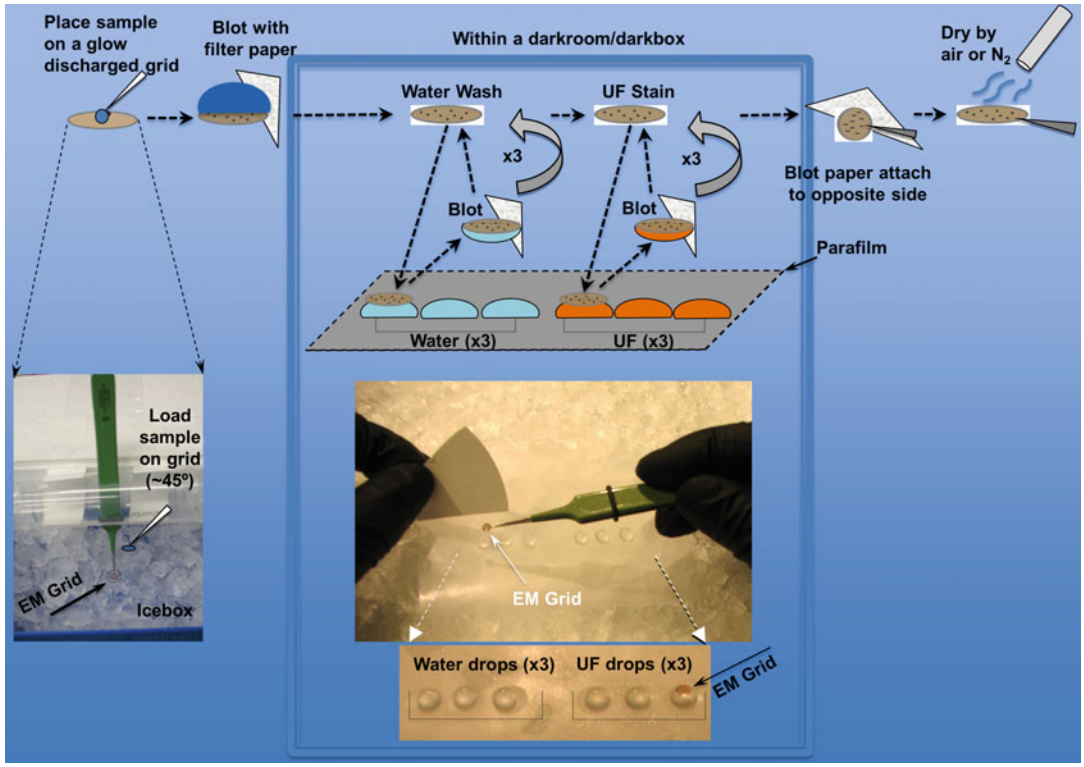

Fig. 2 Diagram of the OpNS protocol procedure. EM grid manipulations with staining reagent, filter paper, and water contacts in chronological order (top cartoon), grid in ice box incubation at 4 °C (left bottom), rapidly contact with stain or water from Parafilm in flat icebox chamber (middle top), three drops of water are added followed by three drops of staining reagent being added on Paraffin film in flat icebox chamber with EM grid lying on top of the last UF staining drop (middle bottom). Notably, the operation must be performed under low-illumination condition. Adapted from refs. 12 and 28

6. Parafilm: 4″ × 4″.
7. Ice.
8. Cu-300 CN: Thin carbon-coated 300 mesh copper grids (Pacific Grid-Tech, San Francisco CA).
9. Dumont Style#5 Medical Tweezers with Clamping ring.
10. Ultrapure water: Obtained from Millipore Synthesis unit.
11. Filter Papers: Qualitative circles, 90 mm (Whatman).

Fig. 1 (continued) DNA-nanogold (**I**) obtained by EM using the optimized negative-staining protocol. Micrographs by EM for all specimens (**A–I**) mentioned above are shown by survey view (left), selected individual particles (middle) and zoom-in particles (right). Bar = 20 nm (left), 5 nm (middle), 2 nm (right), except **h**, in which bars are 40 nm (left), 20 nm (middle), and 10 nm (right). Adapted from refs. 11, 12, 30, 36, 37, 41, 48 and 50

12. Aluminum foil.
13. Petri dishes.
14. EMS 100: Glow discharge unit.
15. Icebox: 4″ × 5″, with lid, insulated.
16. Flat Ice Chamber: Leveled, insulated, uniformly flat, large enough to hold the 4″ × 4″ Parafilm, and contains a lid.

3 Methods

1. Prepare 100 mL of a 1% (w/v) solution of UF powder in deionized water and stir it overnight in a dark room at room temperature, and then store the stock solution in a bottle covered with aluminum foil.
2. Filter 5 mL of the 1% solution with the NORM-JECT syringe and the filter of 0.02 μm, and aliquot it into 2 mL vials, wrapped in aluminum foil to keep the solution in the dark. Immediately after aliquoting the 1% UF solution, place the vials into liquid nitrogen by using a long handle forceps (*see* **Notes 1** and **2**). Store the 2 mL vials of the 1% UF solution in an −80 °C freezer until the usage.
3. Before use, thaw a vial in a 4 °C water bath, and make sure it remains wrapped (cover it) in aluminum foil to keep the vial in the dark.
4. Once the UF solution is thawed and in liquid form, filter the UF solution again, using a 1 mL NORM-JECT syringe and the Anotop filter of 0.02 μm pore size, then cover the vial containing filtered solution with aluminum foil and store it on ice or at 4 °C (*see* **Note 2**).
5. Place a piece of Paraffin film on ice in a uniformly leveled manner into the flat ice chamber, and cover it with aluminum foil.
6. Designate three rows of six small circular regions in a piece of Paraffin film and then place ~35 μL drops of deionized water in the left three circle regions in each row. Subsequently place ~35 μL drops of the filtered UF in the right three small circle regions in each row (*see* **Note 3**).
7. Fill the icebox with ice, cover the icebox, and let it standing for ~10 min.
8. Obtain carbon-coated grids with Dumont™ #5 medical tweezers with clamping ring, perform glow discharge with an EMS 100, and place the grids on a clean filter paper in a petri dish and cover the grids (*see* **Note 4**).
9. Open the icebox and hold the grid with tweezers at a 45° angle at one inch above the surface; place ~3 μL of the lipoprotein sample on the grid and incubate for 1 minute (*see* **Note 5**).

10. Since the UF solutions are light sensitive and unstable, the following **steps 11–14** of operation must be performed in the dark.
11. After ~1 min, remove the excess amount of solution by gently touching the edge of the grid with filter paper. Wash the grid by briefly by placing the surface of the grid with a drop (~35 μL) of deionized water on Parafilm and then blot the grid with filter paper to remove the excessive amount of the solution. The touching and blotting steps are performed three times quickly, and each step is washed with a clean drop of deionized water.
12. Perform the same touching and blotting steps with three successive drops (~35 μL) of 1% UF solution applied on Parafilm, and incubate for 10 s, then remove the excess amount of solution by blotting with water. Gently dip the grid with the last UF drop with the sample side of the grid facing down for 1–3 min in the dark (close the lid of the flat ice chamber) before removing the excess amount of staining reagent by blotting again with the entire backside parallel to the grid (noncarbon side) with filter paper. Subsequently, air-dry the sample by a low-flow of nitrogen gas at room temperature (*see* Fig. 2, **Note 6**).
13. Store the grid on filter paper in a petri dish and partially cover it for ~30 min.
14. Send the grid to EM or store it in a grid storage box (*see* **Note 7**).

4 Notes

1. UF is sensitive to light, so this step of procedure should be performed in the dark. UF is also radioactive and should be handled accordingly under the safety guidance at the Institute. The waste of the UF should be placed in an appropriate waste container in compliance with the appropriate waste management system guidelines of the lab.
2. During filtration, filter the solution very slowly, and ensure that the UF is covered by aluminum foil. Be careful to use the correct side of the filter when it is attached to the syringe. Discard the filter and the syringe as radioactive waste components.
3. Ensure that the Parafilm is leveled when placing it into the flat ice chamber. Use paperweights as necessary to hold the Parafilm down onto the ice. Make circles/wells with care and do not place them too close to each other. Rows of circles should be made according to the number of samples, while having a few extra ones is always best practice in case of any. Divide circles into two sections of three, one is for water, and the other one is for UF. Again, UF is light sensitive, so close the lid whenever possible.

4. Before handling carbon-coated grids, clean the tweezers by lightly wiping them on unused filter paper. Handle grids with tweezers so that the tweezers grip the metal edge of the grid. Do not bend grids, and ensure carbon-coated sides of grids are always faced up. Refer to your instrument manual to perform the glow discharge appropriately with the EMS 100. Alternate glow dischargers or plasma cleaners may be used. Be careful not to clamp down too hard on grids, as they bend easily.
5. Ensure the sample (protein portion) concentration is ~0.005–0.01 mg/mL, and use Dulbecco's phosphate buffered saline to dilute if necessary. When placing a sample on the grid, be careful to approach the grid at an angle and close lid when possible in an icebox to slow down any reactivity of the grid with air (hence the low temperature placement of the grid at ~4 °C or less). Multiple grids can be held at a time in an icebox if desired, but contacting with ice must be avoided at all times.
6. Prepare filter papers beforehand, and cut them into small sections to avoid confusion, and designate one paper for water, and one for UF. Properly discard UF-contaminated paper according to lab guidelines. Be extremely careful to blot the grid by touching the side of grid with filter paper, and ensure the carbon side of the grid is contacting deionized water, and UF stain. Above operations must be performed in the dark since the UF solutions are light sensitive and unstable. It is important to note that the thickness of the stain of the carbon-coated grid is not even. In some areas, the stain is thicker than in other areas. However, the best images of proteins have generally been obtained from areas of thicker staining (Fig. 3). An area of thicker stain looks like a "cloud" on the grid at low magnification (<400×).
7. For storage of the grids, excess heat, dryness, and high humidity conditions must be avoided.

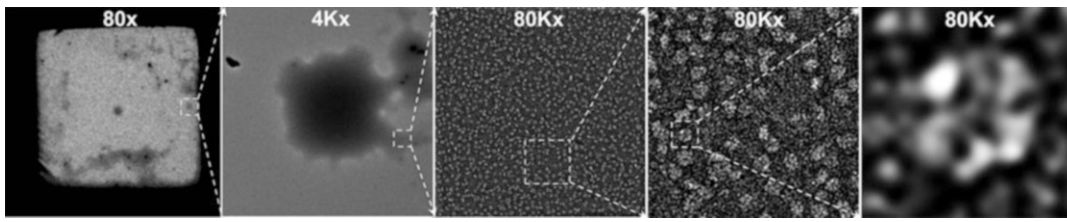

Fig. 3 The best EM imaging area. The best imaging areas of the protein are generally the ones containing thick staining. Micrographs showing cloudy areas are likely the locations to obtain EM images for lipoproteins. Cloud areas designating lipoprotein's locations are highlighted in a box at 80× magnification (left), same designated area is further magnified at 4K× (the second from the left), and 80K× (middle), it is zoomed in at 80K× (the second from the right) and further zoomed in to a single particle scale (right). Adapted from refs. 11, 12, 28 and 29

Acknowledgments

We thank Drs. Ron Krauss, Paul Alivisatos, Haijun Sun, Xiayang Qiu, Lei Zhang, and Mark Garewal, for providing the samples, preparing the EM samples, or preparing the draft. This work was supported by the National Heart, Lung, and Blood Institute of the National Institutes of Health (R01HL115153, 2R01HL115153-06, and R01GM104427,). *Work at the Molecular Foundry was supported by the Office of Science, Office of Basic Energy Sciences of the U.S. Department of Energy under Contract No. DE-AC02-05CH11231.*

References

1. Reichow SL, Gonen T (2009) Lipid-protein interactions probed by electron crystallography. Curr Opin Struct Biol 19:560–565. https://doi.org/10.1016/j.sbi.2009.07.012
2. Gennis RB, Jonas A (1977) Protein-lipid interactions. Annu Rev Biophys Bioeng 6:195–238
3. Gonen T, Cheng YF, Sliz P et al (2005) Lipid-protein interactions in double-layered two-dimensional AQPO crystals. Nature 438:633–638. https://doi.org/10.1038/nature04321
4. Liao M, Cao E, Julius D et al (2013) Structure of the TRPV1 ion channel determined by electron cryo-microscopy. Nature 504:107–112. https://doi.org/10.1038/nature12822
5. Herzik MA Jr, Wu M et al (2017) Achieving better-than-3-A resolution by single-particle cryo-EM at 200 keV. Nat Methods 14:1075–1078. https://doi.org/10.1038/nmeth.4461
6. Orlova EV, Sherman MB, Chiu W et al (1999) Three-dimensional structure of low density lipoproteins by electron cryomicroscopy. Proc Natl Acad Sci U S A 96:8420–8425
7. Ren G, Rudenko G, Ludtke SJ et al (2010) Model of human low-density lipoprotein and bound receptor based on CryoEM. Proc Natl Acad Sci U S A 107:1059–1064. https://doi.org/10.1073/pnas.0908004107
8. Kumar V, Butcher SJ, Oorni K et al (2011) Three-dimensional cryoEM reconstruction of native LDL particles to 16 Angstrom resolution at physiological body temperature. PLoS One 6:e18841. https://doi.org/10.1371/journal.pone.0018841
9. Ludtke SJ, Baldwin PR, Chiu W (1999) EMAN: semiautomated software for high-resolution single-particle reconstructions. J Struct Biol 128:82–97
10. Frank J, Radermacher M, Penczek P et al (1996) SPIDER and WEB: processing and visualization of images in 3D electron microscopy and related fields. J Struct Biol 116:190–199
11. Zhang L, Song J, Newhouse Y et al (2010) An optimized negative-staining protocol of electron microscopy for apoE4 POPC lipoprotein. J Lipid Res 51:1228–1236
12. Zhang L, Song J, Cavigiolio G et al (2011) Morphology and structure of lipoproteins revealed by an optimized negative-staining protocol of electron microscopy. J Lipid Res 52:175–184
13. Ohi M, Li Y, Cheng Y et al (2004) Negative staining and image classification – powerful tools in modern electron microscopy. Biol Proced 6:23–34
14. Oliver RM (1973) Negative stain electron microscopy of protein macromolecules. Methods Enzymol 27:616–672
15. Woeste S, Demchick P (1991) New version of the negative stain. Appl Environ Microbiol 57:1858–1859
16. Bradley DE (1962) A study of the negative staining process. J Gen Microbiol 29:503–516
17. Cunningham WP, Staehelin LA, Rubin RW et al (1974) Effects of phosphotungstate negative staining on the morphology of the isolated Golgi apparatus. J Cell Biol 62:491–504
18. Egelman EH, Amos LA (2009) Electron microscopy of helical filaments: rediscovering buried treasures in negative stain. BioEssays 31:909–911
19. Melchior V, Hollingshead CJ, Cahoon ME (1980) Stacking in lipid vesicle-tubulin mixtures is an artifact of negative staining. J Cell Biol 86:881–884

20. Zhang L, Ren G (2012) IPET and FETR: experimental approach for studying molecular structure dynamics by cryo-electron tomography of a single-molecule structure. PLoS One 7:e30249. https://doi.org/10.1371/journal.pone.0030249
21. Segrest JP, Jones MK, Catte A et al (2015) Surface density-induced pleating of a lipid monolayer drives nascent high-density lipoprotein assembly. Structure 23:1214–1226. https://doi.org/10.1016/j.str.2015.05.010
22. Ghosh M, Ren G, Simonsen JB et al (2014) Cationic lipid nanodisks as an siRNA delivery vehicle. Biochem Cell Biol 92:200–205. https://doi.org/10.1139/bcb-2014-0027
23. Ikon N, Shearer J, Liu J et al (2017) A facile method for isolation of recombinant human apolipoprotein A-I from *E. coli*. Protein Expr Purif 134:18–24. https://doi.org/10.1016/j.pep.2017.03.015
24. Jones MK, Zhang L, Catte A (2010) Assessment of the validity of the double superhelix model for reconstituted high density lipoproteins: a combined computational-experimental approach. J Biol Chem 285:41161–41171. https://doi.org/10.1074/jbc.M110.187799
25. Chen B, Ren X, Neville T et al (2009) Apolipoprotein AI tertiary structures determine stability and phospholipid-binding activity of discoidal high-density lipoprotein particles of different sizes. Protein Sci 18:921–935. https://doi.org/10.1002/pro.101
26. Zhang M, Lei D, Peng B et al (2017) Assessing the mechanisms of cholesteryl ester transfer protein inhibitors. Biochim Biophys Acta 1862:1606–1617. https://doi.org/10.1016/j.bbalip
27. Zhang M, Charles R, Tong H et al (2015) HDL surface lipids mediate CETP binding as revealed by electron microscopy and molecular dynamics simulation. Sci Rep 5:8741. https://doi.org/10.1038/srep08741
28. Rames M, Yu Y, Ren G (2014) Optimized negative staining: a high-throughput protocol for examining small and asymmetric protein structure by electron microscopy. J Vis Exp 90:e51087. https://doi.org/10.3791/51087
29. Zhang L, Tong H, Garewal M et al (2013) Optimized negative-staining electron microscopy for lipoprotein studies. Biochim Biophys Acta 1830:2150–2159. https://doi.org/10.1016/j.bbagen.2012.09.016
30. Zhang L, Yan F, Zhang S et al (2012) Structural basis of transfer between lipoproteins by cholesteryl ester transfer protein. Nat Chem Biol 8:342–349. https://doi.org/10.1038/nchembio.796
31. Zhang M, Zhai X, Li J et al (2018) Structural basis of the lipid transfer mechanism of phospholipid transfer protein (PLTP). Biochim Biophys Acta 1863:1082–1094. https://doi.org/10.1016/j.bbalip.2018.06.001
32. Yu Y, Kuang YL, Lei D et al (2016) Polyhedral 3D structure of human plasma very low density lipoproteins by individual particle cryo-electron tomography1. J Lipid Res 57:1879–1888. https://doi.org/10.1194/jlr.M070375
33. Ren G, Zhang S, Cavigiolio G et al (2010) Cholesteryl ester transfer protein penetrates lipoproteins for cholesteryl ester transfer. Biophys J 98:36a
34. Ercius P, Alaidi O, Rames MJ (2015) Electron tomography: a three-dimensional analytic tool for hard and soft materials research. Adv Mater 27:5638–5663. https://doi.org/10.1002/adma.201501015
35. Lei D, Rames M, Zhang X et al (2016) Insights into the tunnel mechanism of cholesteryl ester transfer protein through all-atom molecular dynamics simulations. J Biol Chem 291:14034–14044. https://doi.org/10.1074/jbc.M116.715565.37
36. Lei D, Marras AE, Liu J et al (2018) Three-dimensional structural dynamics of DNA origami Bennett linkages using individual-particle electron tomography. Nat Commun 9:592. https://doi.org/10.1038/s41467-018-03018-0
37. Zhang L, Lei D, Smith JM et al (2016) Three-dimensional structural dynamics and fluctuations of DNA-nanogold conjugates by individual-particle electron tomography. Nat Commun 7:11083. https://doi.org/10.1038/ncomms11083
38. Liu J, Li H, Zhang L et al (2016) Fully mechanically controlled automated electron microscopic tomography. Sci Rep 6:29231. https://doi.org/10.1038/srep29231
39. Deng X, Qin X, Chen L et al (2016) Large conformational changes of insertion 3 in human glycyl-tRNA synthetase (hGlyRS) during catalysis. J Biol Chem 29:5740–5752. https://doi.org/10.1074/jbc.M115.679126
40. Lu Z, Reddy MV, Liu J et al (2016) Molecular architecture of contactin-associated protein-like 2 (CNTNAP2) and its interaction with contactin 2 (CNTN2). J Biol Chem 291:24133–24147. https://doi.org/10.1074/jbc.M116.748236
41. Lu Z, Wang Y, Chen F et al (2014) Calsyntenin-3 molecular architecture and interaction with neurexin 1alpha. J Biol Chem

289:34530–34542. https://doi.org/10.1074/jbc.M114.606806

42. Cho WJ, Shin L, Ren G et al (2009) Structure of membrane-associated neuronal SNARE complex: implication in neurotransmitter release. J Cell Mol Med 13:4161–4165. https://doi.org/10.1111/j.1582-4934.2009.00895.x
43. Cho WJ, Ren G, Lee JS et al (2009) Nanoscale 3D contour map of protein assembly within the astrocyte porosome complex. Cell Biol Int 33:224–229. https://doi.org/10.1016/j.cellbi.2008.11.008
44. Cho WJ, Ren G, Jena BP (2008) EM 3D contour maps provide protein assembly at the nanoscale within the neuronal porosome complex. J Microsc 232:106–111. https://doi.org/10.1111/j.1365-2818.2008.02088.x
45. Zhang L, Ren G (2010) Determining the dynamic protein structure by individual-particle electron tomography: an individual antibody structure at a nanometer resolution. Biophys J 98:441a
46. Zhang L, Kaspar A, Woodnutt G et al (2010) Monitoring the structural changes of conjugated antibodies by high-resolution electron microscopy and individual-particle electron tomography. Biophys J 98:440a–441a
47. Zhang X, Zhang L, Tong H et al (2015) 3D structural fluctuation of IgG1 antibody revealed by individual particle electron tomography. Sci Rep 5:9803. https://doi.org/10.1038/srep09803
48. Tong H, Zhang L, Kaspar A et al (2013) Peptide-conjugation induced conformational changes in human IgG1 observed by optimized negative-staining and individual-particle electron tomography. Sci Rep 3:1089. https://doi.org/10.1038/srep01089
49. Zhang L, Ren G (2012) High-resolution single-molecule structure revealed by electron microscopy and individual particle electron tomography. J Phys Chem B 2. https://doi.org/10.4172/2161-0398.1000e103
50. Jay J, Bray B, Qi Y et al (2018) IgG antibody 3D structures and dynamics. Antibodies 7:18. https://doi.org/10.3390/antib7020018
51. Zhang HM, Li C, Lei M et al (2017) Structural and functional characterization of a hole-hole homodimer variant in a "knob-into-hole" bispecific antibody. Anal Chem 89:13494–13501. https://doi.org/10.1021/acs.analchem.7b03830